

Supporting Information for the Article: Collective Directional Locking of Colloidal Monolayers on a Periodic Substrate

Ralph L. Stoop,¹ Arthur V. Straube,^{2,3,1} Tom H. Johansen,^{4,5} and Pietro Tierno^{1,6,7,*}

¹*Departament de Física de la Matèria Condensada, Universitat de Barcelona, Barcelona, Spain*

²*Department of Mathematics and Computer Science, Freie Universität Berlin, Berlin, Germany*

³*Group “Dynamics of Complex Materials”, Zuse Institute Berlin, Berlin, Germany*

⁴*Department of Physics, University of Oslo, P. O. Box 1048 Blindern, 0316 Oslo, Norway*

⁵*Institute for Superconducting and Electronic Materials,*

University of Wollongong, Northfields Avenue, Wollongong, NSW 2522, Australia

⁶*Universitat de Barcelona Institute of Complex Systems (UBICS), Universitat de Barcelona, Barcelona, Spain*

⁷*Institut de Nanociència i Nanotecnologia, IN²UB, Universitat de Barcelona, Barcelona, Spain.*

MAGNETIC FIELD ABOVE THE SUBSTRATE

The total magnetic field \mathbf{H} above the bubble-pattern ferrite garnet film (FGF) is determined by the externally applied time-alternating field \mathbf{H}^{ext} and the stray field of the substrate \mathbf{H}^{sub} , as given by their superposition,

$$\mathbf{H}(\mathbf{r}, t) = \mathbf{H}^{\text{ext}}(t) + \mathbf{H}^{\text{sub}}(\mathbf{r}, t). \quad (\text{S1})$$

The ac component of the field has elliptic polarization,

$$\mathbf{H}^{\text{ext}}(t) \equiv (-H_x \sin \omega t, 0, H_z \cos \omega t), \quad (\text{S2})$$

with $H_x = H_0 \sqrt{1 + \beta}$, $H_z = H_0 \sqrt{1 - \beta}$ and the ellipticity β . Here, H_0 and ω are the amplitude and angular frequency of modulation.

The main difficulty is the evaluation of \mathbf{H}^{sub} . Although the exact solution is available, it is too cumbersome. To gain qualitative physical insights, we therefore resort to a much simpler approximation.

Exact solution

To calculate \mathbf{H}^{sub} exactly, we sum up the field from a triangular lattice with period a of magnetic bubbles with lattice vectors $\mathbf{p} = n\mathbf{a}_- + m\mathbf{a}_+$, with $\mathbf{a}_\pm := (\sqrt{3}a/2, \pm a/2)$, and n, m integers. Each bubble is considered as a cylindrical uniformly magnetized ferromagnetic domain [1], generating a stray field above its surface, which can be written in cylindrical (r, z) coordinates as $\mathbf{h} = \mathbf{e}_r h_r(r, z, t) + \mathbf{e}_z h_z(r, z, t)$, where

$$h_r = \frac{M_s}{\pi} \sqrt{\frac{D}{2r}} Q_{\frac{1}{2}} \left(\frac{r^2 + D^2/4 + z^2}{rD} \right), \quad (\text{S3a})$$

$$h_z = M_s - \frac{M_s}{\pi} [\kappa_- \Pi(n_+ | K) + \kappa_+ \Pi(n_- | K)]. \quad (\text{S3b})$$

Here, M_s is the saturation magnetization, $\mathbf{e}_r = (x - p_x)\hat{\mathbf{x}}/r + (y - p_y)\hat{\mathbf{y}}/r$, $r = \sqrt{(x - p_x)^2 + (y - p_y)^2}$, Q_n is the Legendre function of the second kind and order n , $\Pi(n, m)$ gives the complete elliptic integral of the third kind, $K = \sqrt{2rD/[z^2 + (r + D/2)^2]}$; $D(t) = 2a\sqrt{(H_z^{\text{ext}}(t)/M_s + 1) \sin(\pi/3)/2\pi}$, $n_\pm = 2r/(r \pm$

$\sqrt{r^2 + z^2}$), and $\kappa_\pm = (\sqrt{r^2 + z^2} \pm D/2)(\sqrt{r^2 + z^2} \pm r)/(z\sqrt{(r + D/2)^2 + z^2})$.

The field generated by such array is given by $\mathbf{H}_b = \sum_{n,m} \mathbf{h}_{nm}$ with the indexes n and m over the entire triangular lattice. The substrate field is obtained as the superposition $\mathbf{H}^{\text{sub}}(\mathbf{r}) := \mathbf{H}_b - \mathbf{H}_f$, where \mathbf{H}_f is the contribution due to the oppositely magnetized film calculated for a cylindrical domain covering the entire sample area. Note that solution (S3) can be alternatively expressed in integral form [2] rather than using the Legendre functions and elliptic integrals, which are formally equivalent representations.

Simplified solution

The realistic distribution of magnetization $M(x, y)$ is extremely sharp, leading to a highly cumbersome solution for the substrate field [see Eq. (S3) and eventual expression for $\mathbf{H}^{\text{sub}}(\mathbf{r})$] and impeding analytic treatment. A much more tractable solution is obtained by considering a simplified “smooth and soft” hexagonal distribution $M(x, y) = M_s \sum_{i=0}^2 \cos(\mathbf{k}_i \cdot \mathbf{r})$ with the wave vectors $\mathbf{k}_0 = k\hat{\mathbf{x}}$, $\mathbf{k}_1 = k(\hat{\mathbf{x}} + \sqrt{3}\hat{\mathbf{y}})/2$, $\mathbf{k}_2 = k(\hat{\mathbf{x}} - \sqrt{3}\hat{\mathbf{y}})/2$ and $k = 4\pi/(\sqrt{3}a)$. The stray field $\mathbf{H}^{\text{sub}}(\mathbf{r})$ above the FGF ($z > 0$) satisfies the Laplace equation, $\nabla^2 \mathbf{H}^{\text{sub}} = 0$, along with the periodicity conditions and the requirement $H_z^{\text{sub}}(x, y, z \rightarrow 0) = M(x, y)$. Solving this boundary value problem yields

$$\mathbf{H}^{\text{sub}}(x, y, z) = M_s e^{-kz} \mathbf{h}^{\text{sub}}(x, y) \quad (\text{S4})$$

with the field components $h_x^{\text{sub}}(\mathbf{r}) = \sum_{i=0}^2 a_i \sin(\mathbf{k}_i \cdot \mathbf{r})$, $h_y^{\text{sub}}(\mathbf{r}) = \sum_{i=0}^2 b_i \sin(\mathbf{k}_i \cdot \mathbf{r})$, $h_z^{\text{sub}}(\mathbf{r}) = \sum_{i=0}^2 \cos(\mathbf{k}_i \cdot \mathbf{r})$, where $a_0 = 1$, $a_1 = a_2 = 1/2$, $b_0 = 0$, $b_1 = -b_2 = \sqrt{3}/2$.

At a given elevation z above the FGF the total field is

$$\begin{aligned} \mathbf{H}(\mathbf{r}, t) &= \mathbf{H}^{\text{ext}}(t) + \mathbf{H}^{\text{sub}}(\mathbf{r}) \\ &= H_0[\mathbf{h}^{\text{ext}}(t) + \alpha \mathbf{h}^{\text{sub}}(x, y)], \end{aligned} \quad (\text{S5})$$

where $H^{\text{sub}}/H^{\text{ext}} \simeq \alpha := M_s e^{-kz}/H_0$. Similarly to the stripe-patterned FGF setup [3], the elevation of the particle above the film surface $z \simeq a$. As a result, for the typical experimental conditions $0 < \alpha < 1$.

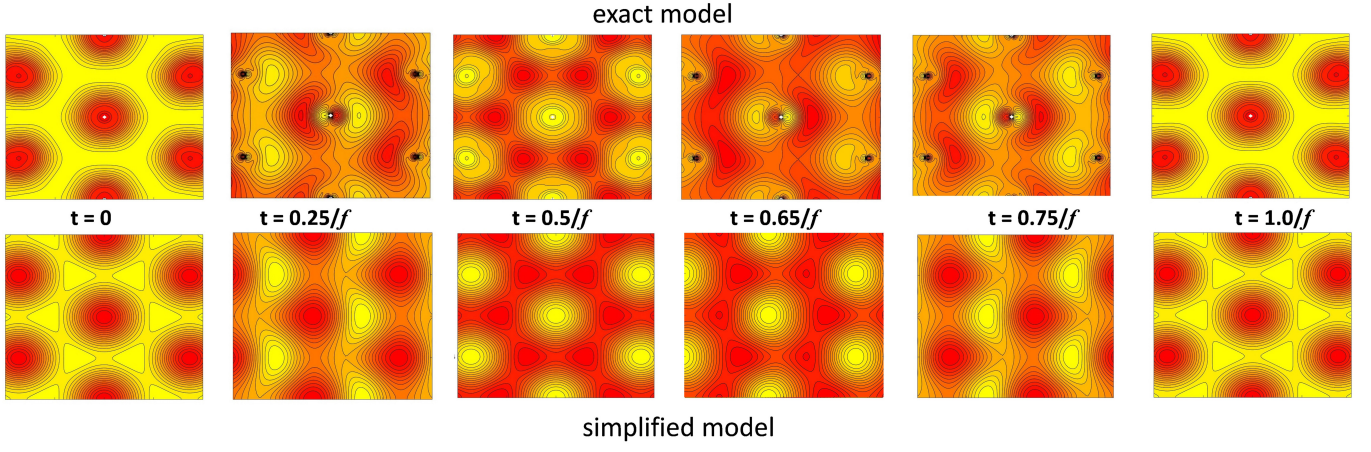


FIG. S1. Evolution over a time period of the single particle potential (S6) from the exact model based on solution (S3) (top), and the approximate potential from the simplified model, Eq. (S7).

SIMPLIFIED MAGNETIC LANDSCAPE AND DIPOLAR INTERACTIONS

Here we utilize an approximate analytic solution based on Eq. (S4) to put forward a simplified theoretical model. It helps guessing physical mechanisms underlying directional locking observed in the experiment. In particular, the model explains the mean drift of particles and suggests what interaction governs the assembly and alignment of particles along the crystallographic directions. We note that our model neglects hydrodynamic interactions suggesting that magnetic forces dominate the dynamics of the system.

Dynamics of individual particles

A spherical paramagnetic particle of volume V and effective magnetic susceptibility χ polarizes in the magnetic field \mathbf{H} , acquiring an induced magnetic moment $\mathbf{m} = \chi V \mathbf{H}$. The energy of interaction of the induced dipole with the field above the substrate reads

$$U_s(\mathbf{r}, t) = -\frac{1}{2}\mu_0(\mathbf{m} \cdot \mathbf{H}) = -\frac{1}{2}\mu_0\chi V \mathbf{H}^2(\mathbf{r}, t), \quad (\text{S6})$$

where $\mu_0 = 4\pi \times 10^{-7} \text{ H m}^{-1}$ is the magnetic permeability of free space. If α in Eq. (S5) is small enough, potential (S6) can be approximated as

$$U_s(x, y, t) \approx -U_0 \mathbf{h}^{\text{ext}}(t) \cdot \mathbf{h}^{\text{sub}}(x, y) \quad (\text{S7})$$

with the characteristic energy $U_0 = \mu_0\chi V H_0 M_s e^{-kz}$.

Comparison of the exact and approximate potentials is given in Figs. S1 and S2 (with the frequency $f = \omega/(2\pi)$), which manifest their qualitative similarity. Note that the potentials display the same morphology in a wide range of β , where the modulation remains essentially elliptical. The typical picture of individual Brownian motion

in potential (S7) reflects the mean speed observed in the experiment, see Fig. S3. The value of ellipticity is set to $\beta = -1/3$ and the period of lattice is chosen to be close to the experimental value, $a = 3.2 \mu\text{m}$. The characteristic frequency $f_0 (\propto U_0) \approx 4.2 \text{ Hz}$ defines the transition from the running to sliding dynamic states and the free diffusivity D_0 softens the transition. For the mean drift along the y direction, the modulation field as in Eq. (S2) is to be replaced with the expression $\mathbf{H}^{\text{ext}}(t) = (0, -H_y \sin \omega t, H_z \cos \omega t)$ with $H_y = H_x = H_0 \sqrt{1 + \beta}$.

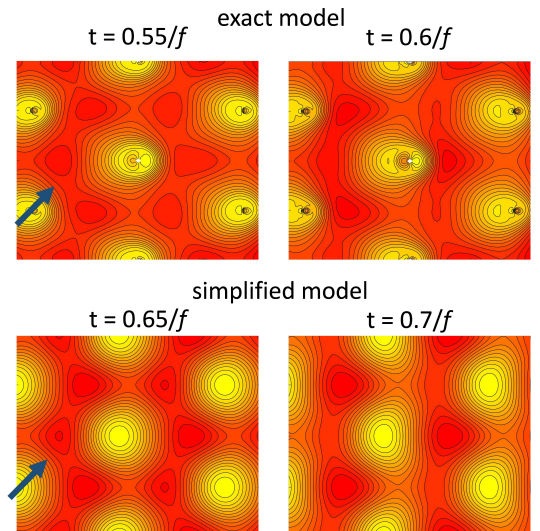


FIG. S2. Snapshots of the energy landscape from the exact model based on solution (S3) (top) and from the simplified model, Eq. (S7) (bottom) and calculated for two instant of times. The blue arrows in the two images at the left indicate the minima along the $-1 - 1$ direction which disappear after $t = 0.5/f$.

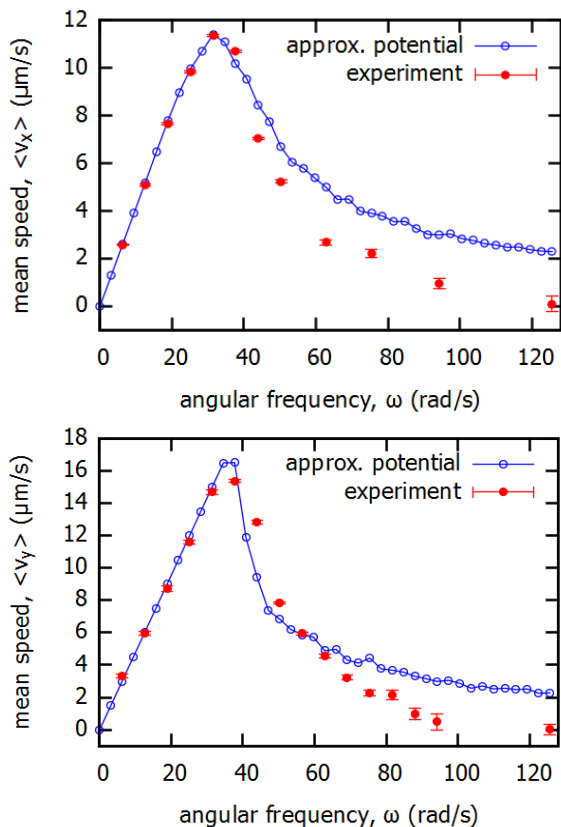


FIG. S3. Mean speeds of a Brownian particle $\langle v_x \rangle$ (top) and $\langle v_y \rangle$ (bottom) corresponding to potential (S7) for the modulation in the (x, z) - and (y, z) -planes, respectively. Parameters are $\beta = -1/3$, $\lambda = 3.2 \mu\text{m}$, $\omega_0 = 2\pi f_0 = 26.5 \text{ rad/s}$ and $D_0 = 0.05 \mu\text{m}^2/\text{s}$.

Magnetic interaction of particles

Magnetic interaction of dipoles \mathbf{m}_1 and \mathbf{m}_2 at positions \mathbf{r}_1 and \mathbf{r}_2 are described by the pairwise dipolar potential $U_d(\mathbf{r}_1, \mathbf{r}_2) = \mu_0[(\mathbf{m}_1 \cdot \mathbf{m}_2) - 3(\hat{\mathbf{r}}_{12} \cdot \mathbf{m}_1)(\hat{\mathbf{r}}_{12} \cdot \mathbf{m}_2)]/(4\pi r_{12}^3)$, where $\mathbf{r}_{12} = \mathbf{r}_1 - \mathbf{r}_2$, $r_{12} = |\mathbf{r}_{12}|$, and $\hat{\mathbf{r}}_{12} = \mathbf{r}_{12}/r_{12}$. For induced dipoles, this leads us to

$$U_d(\mathbf{r}_1, \mathbf{r}_2) \propto \frac{(\mathbf{H}_1 \cdot \mathbf{H}_2) - 3(\hat{\mathbf{r}}_{12} \cdot \mathbf{H}_1)(\hat{\mathbf{r}}_{12} \cdot \mathbf{H}_2)}{r_{12}^3} \quad (\text{S8})$$

with $\mathbf{H}_1 = \mathbf{H}(\mathbf{r}_1, t)$ and $\mathbf{H}_2 = \mathbf{H}(\mathbf{r}_2, t)$ given by Eq. (S5). For small α , the leading term in Eq. (S5) reads $\mathbf{H}(\mathbf{r}, t) \approx \mathbf{H}^{\text{ext}}(t) = H_0 \mathbf{h}^{\text{ext}}(t)$. Applied to Eq. (S8) it generally describes assembly of particles into chains in the plane of modulation, i.e. along the x -direction, see Eqs. (34) and (35) in Ref. [4]. At $\beta = -1/3$, however, the particles become noninteracting along the x -direction and weakly repulsive in all other directions.

To look for any non vanishing effect, we account for the next term in Eq. (S5), leading to cross terms of order $O(\alpha)$ in potential (S8). Further, motivated by experimental observation, we consider a pair of particles

separated by the lattice constant a and aligned along a crystallographic axis, $\mathbf{a}_{\pm} = (\sqrt{3}a/2, \pm a/2)$. Thus, by putting the coordinates of particles as $x_2 = x_1 \pm \sqrt{3}a/2$ and $y_2 = y_1 \pm a/2$, where any of four sign combinations are possible, Eq. (S8) is simplified to

$$U_d(\mathbf{r}_1) \propto \frac{F_{xx}(1 - 3\hat{x}_{12}^2) + F_{zz} - 3F_{xy}\hat{x}_{12}\hat{y}_{12}}{r_{12}^3}, \quad (\text{S9})$$

where $F_{xx} = 2H_x^{\text{ext}}(t)H_x^{\text{sub}}(\mathbf{r}_1)$, $F_{xy} = 2H_x^{\text{ext}}(t)H_y^{\text{sub}}(\mathbf{r}_1)$, $F_{zz} = 2H_z^{\text{ext}}(t)H_z^{\text{sub}}(\mathbf{r}_1)$, $\hat{x}_{12} = (x_1 - x_2)/r_{12} = \pm\sqrt{3}/2$, $\hat{y}_{12} = (y_1 - y_2)/r_{12} = \pm 1/2$, and $r_{12} = a$.

The structure of potential (S9) allows us to draw few important conclusions. First, its clear hexagonal structure [e.g., comparison at $t = 0$ with Eq. (S7) shows that $U_d \propto U_s$] indicates that dipolar interactions exhibit attractions along the crystallographic directions and evolve in time. Together with individual propulsion, these interactions suggest the formation of chains aligned and running along the crystallographic axes $(\sqrt{3}a/2, \pm a/2)$, as observed in the experiment. Second, similarly to the mechanism of propulsion, these dipolar interactions are caused by the interplay of the fields of substrate and external modulation, which is qualitatively different to the simple mechanism based on the modulation field [4].

SUPPORTING VIDEOS

With the article we provide 2 video clips as supplements of the figures in the main text.

- **Video1(.WMF):** Dynamics of a dilute monolayer of paramagnetic colloidal particles driven to the left above magnetic bubble lattice characterized by a lattice constant $a = 3.5 \mu\text{m}$. The rotating magnetic field has amplitudes $H_x = 600 \text{ Am}^{-1}$, $H_z = 840 \text{ Am}^{-1}$, which give rise to $H_0 = 720 \text{ Am}^{-1}$ and $\beta = -1/3$, and the angular frequency is $\omega = 25.1 \text{ rads}^{-1}$. The bubbles are visible due to the polar Faraday effect.
- **Video2(.WMF):** Paramagnetic colloids driven through a magnetic bubble lattice under similar field parameters as for the previous movie. Here the magnetic bubbles are not visible due to the absence of polarization elements on the optical path. The particle density ρ increases as time proceeds, and the system transits from a liquid-like phase where individual particles display random movement along the transversal direction, to a directionally locked phase composed by trains of particles sliding along one of the two crystallographic axes -10 and $0-1$. Towards the end of the video, at high density, the particles form a closely packed monolayer that slides linearly across the lattice and the directional locking is lost.

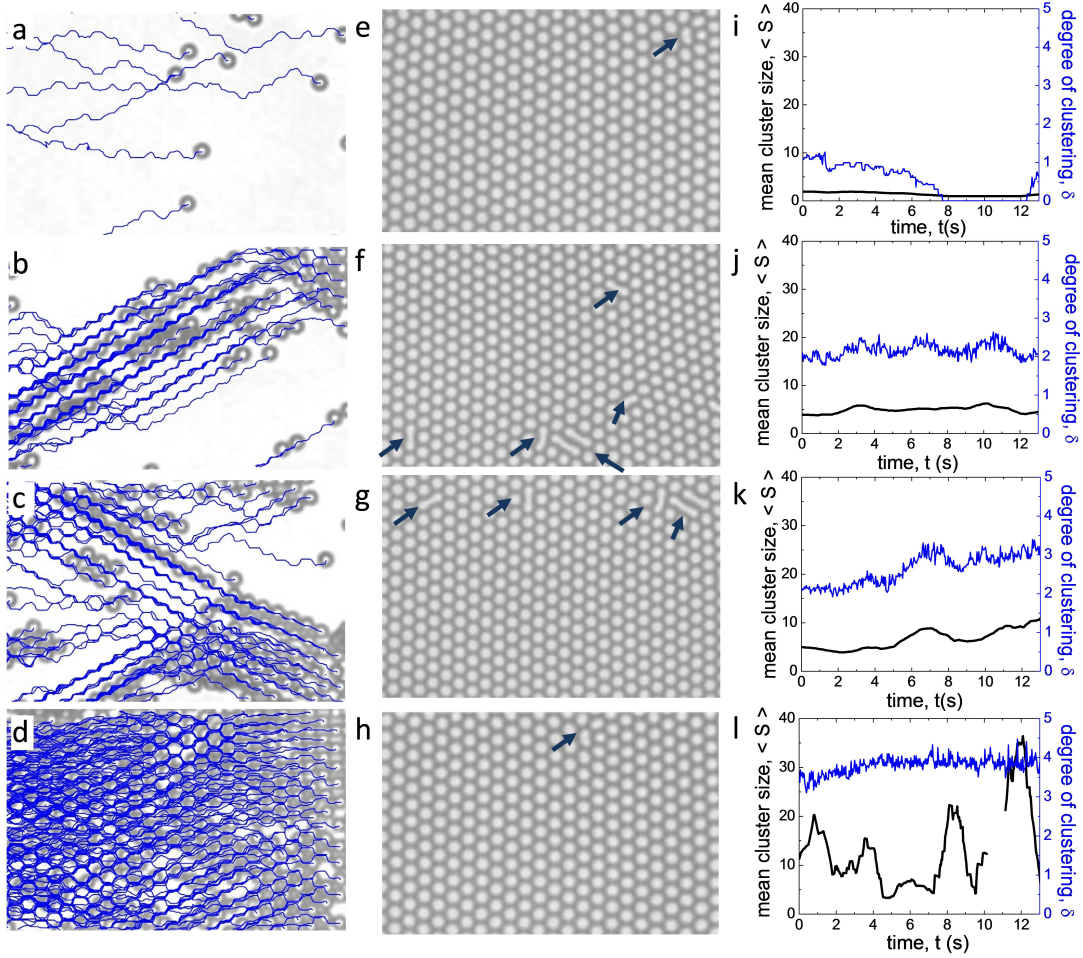


FIG. S4. (a-d) Experimental images with superimposed particle trajectories for four normalized densities: (a) $\rho = 0.02$, (b) $\rho = 0.23$, (c) $\rho = 0.16$ and (d) $\rho = 0.58$. (e-h) Corresponding polarization microscope images showing the underlying magnetic lattice. Point defects in form of double magnetic domains or deformed bubbles are indicated by blue arrows. (i-l) Analysis of the mean cluster size $\langle S \rangle$ and degree of clustering δ calculated for the different experiments.

* ptierno@ub.edu

- [1] W. F. Druyvesteyn, D. L. A. Tjaden and J. W. F. Dorleijn, Philips Res. Repts. **27**, 7 (1972).
- [2] A. Soba, P. Tierno, T. M. Fischer and F. Saguès, Phys. Rev. E **77**, 060401 (2008).
- [3] A. V. Straube, P. Tierno, Europhys. Lett. **103**, 28001 (2013).
- [4] A. V. Straube, P. Tierno, Soft Matter **10**, 3915 (2014).